HHS Public Access

Author manuscript

J Magn Reson. Author manuscript; available in PMC 2018 March 01.

Published in final edited form as:

J Magn Reson. 2017 March ; 276: 31–36. doi:10.1016/j.jmr.2016.12.015.

Imaging Thiol Redox Status in Murine Tumors *In Vivo* with Rapid-scan Electron Paramagnetic Resonance

Boris Epel[1], **Subramanian V. Sundramoorthy**[1], **Martyna Krzykowska-Serda**[1], **Matthew C. Maggio**[1], **Mark Tseytlin**[2], **Gareth R. Eaton**[3], **Sandra S. Eaton**[3], **Gerald M. Rosen**[4], **Joseph P. Y. Kao**[5], and **Howard J. Halpern**[1]

[1]Center for EPR Imaging In Vivo Physiology, Department of Radiation and Cellular Oncology, University of Chicago, IL, USA

[2]Department of Biochemistry, School of Medicine, University of West Virginia, Morgantown, WV, USA 26506

[3]Department of Chemistry and Biochemistry, University of Denver, Denver, CO, USA 80208

[4]Department of Pharmaceutical Sciences, University of Maryland School of Pharmacy, Baltimore, MD, USA 21201

[5]Center for Biomedical Engineering & Technology, and Department of Physiology, University of Maryland School of Medicine, Baltimore, MD, USA 21201

Abstract

Thiol redox status is an important physiologic parameter that affects the success or failure of cancer treatment. Rapid scan electron paramagnetic resonance (RS EPR) is a novel technique that has shown higher signal-to-noise ratio than conventional continuous-wave EPR in *in vitro* studies. Here we used RS EPR to acquire rapid three-dimensional images of the thiol redox status of tumors and normal tissues in living mice. This work presents, for the first time, *in vivo* RS EPR images of the kinetics of the reaction of $^{2}H,^{15}N$-substituted disulfide-linked dinitroxide (PxSSPx) spin probe with intracellular glutathione. The cleavage rate is proportional to the intracellular glutathione concentration. Feasibility was demonstrated in a FSa fibrosarcoma tumor model in C3H mice. Similar to other *in vivo* and cell model studies, decreasing intracellular glutathione concentration by treating mice with L-buthionine sulfoximine (BSO) markedly altered the kinetic images.

Graphical Abstract

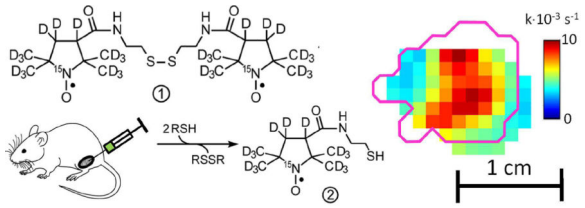

Keywords

electron paramagnetic resonance; thiol redox status; EPR imaging; rapid scan EPR; glutathione

1. Introduction

Clinical evidence suggests that thiol redox status[1–3] is a crucial physiologic endpoint, which may inform redox-status-modulating therapies leading to more successful cancer treatment. The heterogeneity of tumor environmental parameters (e.g., oxygen and pH)[5–9] suggests that physiological imaging could be clinically beneficial. An imaging modality that could define, in an individual patient, the redox status of the tumor microenvironment would allow the selection of individuals who would benefit from local cancer therapies that would rebalance the tumor microenvironment by targeting resistant tumor regions. In contrast, patients whose tumor redox status indicates that such therapies are likely to be ineffective would avoid potentially toxic treatment.

The thiol-disulfide balance determines the intracellular redox microenvironment. This balance is essential for maintaining proper cellular function, and is therefore tightly regulated. Cellular thiols such as glutathione (GSH), and cysteine side chains on proteins (PSH), which coexist with their disulfide counterparts (GSSG and PSSP) comprise the cellular pool of redox-active sulfhydryls. The GSH/GSSG couple constitutes close to half of the thiol/disulfides in the cell and is thus an appropriate measure of thiol/disulfide balance.

In addition to its role in physiological regulation, GSH is also critical in maintaining cell viability by detoxifying xenobiotics that would otherwise compromise cellular function[10–12]. Moreover, GSH is the physiologic cofactor for GSH peroxidases, which reduce hydrogen peroxide and organic hydroperoxides to water and alcohols, respectively[13,14].

Current cancer treatment commonly comprises radiotherapy with ionizing radiation, which generates highly reactive free radicals, and chemotherapy with cytotoxic agents. Cellular thiols can act as cofactors for detoxifying enzymes; therefore they can antagonize both of these therapeutic approaches and thus lead to unsuccessful clinical outcomes[2]. This understanding has led to strategies to control GSH levels in tumor cells and thereby enhance cell killing[2,15,16].

Therefore, the ability to assess the intracellular thiol-disulfide balance is undoubtedly critical in predicting responsiveness of cancers to therapy.

We have recently synthesized a water-soluble, disulfide-linked dinitroxide (hereafter “disulfide-dinitroxide”) in both the normoisotopic and $^{2}H,^{15}N$-substituted forms[4]. In this

report, the term “PxSSPx” designates the $^{2}H,^{15}N$-substituted disulfide-dinitroxide. The disulfide-dinitroxides and the corresponding monomeric forms (generated through cleavage by thiols) have been characterized by EPR spectroscopy at X-band, L-band, and at 250 MHz[4,17]. Importantly, the rate of disulfide cleavage in living cells is markedly decreased after treatment with *L*-buthionine sulfoximine (BSO, a specific inhibitor of GSH biosynthesis), which suggests that the disulfide-dinitroxides could be useful as probes of thiol redox status in vivo. In the present study, we introduce PxSSPx into leg-borne tumors in mice, where intratumoral thiols can cleave the dinitroxide into monomeric forms (Fig. 1), and monitor the local progress of the cleavage reaction with rapid-scan EPR imaging at 250 MHz.

2. Results

2.1. Spectroscopic measurements of murine tumors at 250 MHz

After intratumoral injection, cleavage of PxSSPx into PxSH proceeded rapidly. To capture the initial phase of the cleavage reaction, data acquisition was initiated and then the spin probe was injected *in situ*. The time of injection was determined by post-acquisition inspection of the EPR spectra. Each cycle of data acquisition comprised a 4-second single spectroscopic trace followed immediately by a 31-second 3D rapid-scan (RS) image; this cycle was repeated continuously. The duration of the experiment was ~ 1 h, so that both cleavage and clearance of the spin probe could be captured. Single spectral traces and RS image projections had the same 6mT field sweep that encompassed the full EPR spectra of PxSSPx and its cleavage product.

Fig. 2 shows snapshots of the evolution of the EPR spectrum. The spectrum in Fig. 2A (the open circles), acquired within 30 s after injection, contains primarily the spectroscopic signature of PxSSPx. This interpretation was confirmed by spectral simulation (solid curve in Fig. 2A). The spectrum in Fig. 2B, acquired 175 s after injection, is a superposition of PxSSPx and PxSH spectra. The spectrum in Fig. 2C, acquired after ~30 min post-injection, is attributable to PxSH, as confirmed by spectral simulation (solid trace in Fig. 2C). To enable analysis of kinetics, the spectrum recorded at every time point was decomposed into a weighted superposition of the simulated PxSSPx and PxSH spectra, normalized to the area under the curve. The weighting factors are thus proportional to the detected number of spins. The Hamiltonian parameters for PxSSPx (see the caption of Fig. 2) were taken from the phantom study, while the linewidth was determined from the fitting of the first traces in the time sequence (Fig. 2A). The simulation parameters for PxSH were derived from the traces containing primarily this specie (Fig. 2C). The time dependence of the weighting factors is presented in Fig. 2D: PxSSPx (triangles) decreases monotonically, while PxSH rises initially and then declines.

2.2. Kinetics simulation

PxSSPx and PxSH equilibrate between extracellular and intracellular compartments rapidly relative to the time scale of the experiment[4]; therefore, assuming that cellular thiol concentration, [RSH], remains constant, the time course of cleavage can be analyzed by a simple kinetic model incorporating two processes: 1) cleavage of PxSSPx by intracellular

thiols, which decreases PxSSPx and increases PxSH; and 2) clearance of PxSSPx and PxSH from the detection volume of the resonator. Process 1 is described by Eqs. 1 and 2.

$$S_{\mathrm{PxSSPx}}=S^{0}_{\mathrm{PxSSPx}}e^{-k[\mathrm{RSH}]t} \quad [1]$$

$$S_{\mathrm{PxSH}}=2aS^{0}_{\mathrm{PxSSPx}}(1-e^{-k[\mathrm{RSH}]t}) \quad [2]$$

Here S^{0}_{PxSSPx} is the initial number of PxSSPx molecules; [RSH] is the concentration of glutathione; k is the bimolecular rate constant of PxSSPx cleavage by RSH. Since a number of pathways leading to the disappearing of the observable spins are possible in vivo, we assume that the total number of spins in the outcome of the cleavage reaction is different from S^{0}_{PxSSPx} by a "spin count" factor of $a \leq 1$. The observed cleavage rate constant in the experiment is the pseudo-unimolecular rate constant $k^{obs} = k[\mathrm{RSH}]$. Additional kinetic processes include the clearance of PxSSPx and PxSH. Although the two species could be cleared at somewhat different rates, the nature and quality of the data likely would not permit estimation of two independent rate constants. Therefore, we introduce a single clearance rate constant k^{clr} to arrive at the final formulae for the simplest kinetic model:

$$S_{\mathrm{PxSSPx}}=S^{0}_{\mathrm{PxSSPx}}e^{-(k^{\mathrm{obs}}+k^{\mathrm{clr}})t} \quad [3]$$

$$S_{\mathrm{PxSH}}=aS^{0}_{\mathrm{PxSSPx}}\left(1-e^{-k^{\mathrm{obs}}t}\right)e^{-k^{\mathrm{clr}}t} \quad [4]$$

Table 1 contains the results for 3 representative experiments. As can be seen in all experiments the outcome of cleavage produced a spin count factor $a < 1$. This is different from the in vitro experiment (data not shown) where $a \approx 1$ was observed. A k^{obs} values of $2.0{\cdot}10^{-3}$ s^{-1} to $3{\cdot}10^{-3}$ s^{-1} were observed, while clearance rates of $0.4{\cdot}10^{-3}$ to $1.0{\cdot}10^{-3}$ s^{-1} were typical.

In a separate limited set of spectroscopic measurements, we attempted determination of k^{obs} with injections having 50% and 75% lower spin probe concentration. We observed a slight ($2.85(1.0) \times 10^{-3}$ s^{-1}) decrease in PxSH k^{obs}; however, the lower SNR prevented us from making a conclusive determination of the effect of spin probe concentration on the results.

2.3. Rapid Scan imaging

The imaging parameters were chosen to accommodate rapid signal dynamics. We were not able to perform 4D spectral-spatial imaging, because imaging speed would have been slower by more than 10-fold. A smaller number of image projections (96) further accelerated acquisition. Since 3D imaging focuses on a single point (magnetic field) in the EPR

spectrum, we selected the field position to correspond to the high-field peak (marked with asterisk in Fig. 2C). A 3D image can be reconstructed without artifacts from a narrow and isolated spectral feature. The width of the feature should be small comparable to the line broadening produced by the gradient and other features should not contribute to the EPR spectrum obtained under the gradient. The upper field PxSH spectrum feature marked in Fig. 2C satisfies this requirement when limited gradient strengths are used. The gradient strength below 0.9 mT/cm applied to objects smaller than ~2 cm does not force signals from upper and lower spectral features to overlap (0.9 mT/cm*2 cm < 2.04 mT). The PxSSPx spectrum (Fig. 2A) does not satisfy the above symmetry requirement and thus could not be reliably imaged using 3D methodology. Fortunately, the linewidth of the PxSSPx signal and its high-field features were considerably broader than that of the PxSH spectrum. Moreover the applied gradient did not contribute much to this linewidth and projection filtration used in the image reconstruction process effectively eliminated it from the resulting image., The residual contribution of PxSSPx to spectral intensity was small and thus was neglected. 3D images of PxSH taken every 35 seconds yielded detailed kinetics data in every voxel. Eq. 4 was used to fit the time dependence of voxel intensity.

Fig. 3A shows a representative slice from the cleavage kinetics image; the magenta outline shows the tumor border determined from a registered MRI image. Confinement of the image to the tumor area is consistent with injection of the spin probe directly into the tumor. When the tumors were injected with PxSSPx and imaged, and the same protocol was repeated 6 or 24 h later, the two sequential imaging episodes yielded essentially similar kinetic parameters. The mode of the k^{obs} distribution in the image is somewhat higher than k^{obs} determined from the spectroscopic data, which can be explained by different image fitting procedure that uses Eqn. 4 only.

To test the sensitivity of the methodology to changes in [RSH], imaging was repeated 24 h after treating mice with L-buthionine sulfoximine (BSO). BSO is a highly selective and potent inhibitor of γ-glutamylcysteine synthetase, the rate-limiting enzyme in the GSH biosynthetic pathway, and is thus highly effective in attenuating intracellular GSH levels[18]. Because GSH constitutes a significant fraction of total cellular thiols (Hansen et al. 2009), lowering intracellular GSH concentration is expected to slow the cleavage reaction. Image and rate distributions in Fig. 3B show significantly reduced cleavage rates and, by inference, reduced cellular thiol content. Considerable diminution of spin probe clearance rates after BSO injection was also observed (see Figs. 3C and 3D). When cellular GSH content is markedly decreased by BSO treatment, intracellular cleavage of PxSSPx slows and does not yield PxSH exclusively (as represented in Fig. 1). Rather, the intermediate, PxSSG, can accumulate. But PxSSG, with three charged functional groups in its GSH moiety, is membrane-impermeant and thus trapped in the cell, which would contribute to slowed clearance from the tumor. In separate control experiments where BSO treatment was omitted, essentially similar kinetic parameters were determined from the initial and 24-hour images.

3. Discussion

Signal to noise ratio (SNR) is the major factor that limits EPR imaging. RS EPR is an enhancement of CW methodology[19,20] that offers a solution to this problem. Two key features of RS EPR are direct detection of the EPR signal (no magnetic field modulation) and scanning the complete EPR line at fast rates. Although rapid passage scanning rates were not achieved for the nitroxides used in this study, direct detection and full spectrum magnetic field sweep achieved sufficient enhancement in signal-to-noise ratio (SNR) and reduction of acquisition time relative to CW to enable the imaging of PxSSPx cleavage by thiols in tumor cells.

Spectroscopic results

Spectroscopic results can be interpreted using the rate constant for cleavage of PxSSPx by RSH at 37 °C, estimated from *in vitro* measurements[4]. The bimolecular rate constant is 0.747 $M^{-1}s^{-1}$ at pH 7.2 and 37 °C which, in combination with our observed cleavage kinetics yields an estimate of [RSH] 2.7 to 4.8 mM in untreated control tumors and [RSH] 1.5 to 2.1 mM in BSO-treated tumors. These values may be compared with the value determined in different murine mammary tumors by an essentially similar technique: ~10 mM[21].

Injection of spin probe directly into a tumor has advantages and disadvantages. On one hand, spin probe delivery was very efficient and toxicity was low owing to the low dosage per body weight. On other hand, the procedure was somewhat invasive, and may have had a confounding effect on EPR signal dynamics due to clearance from the region of observation. The invasiveness was reduced by using 30 G needles. In light of the relatively fast kinetics of spectral changes (on the order of 200 s) comparable to the spin probe redistribution time after iv injection, other modes of spin probe delivery are, at this time, impractical.

The analysis of EPR spectra demonstrates that only 40–60% of the overall amount of spin probe is converted to PxSH ($a < 1$). This could be explained by a bioreduction of spin probes or spin probe binding to tissue components and consequent broadening of the spectrum.

Imaging methodology

To accelerate image acquisition to image the kinetics, we had to sacrifice full spectrum 4D spectral-spatial imaging in favor of rapid 3D spatial imaging of a single spectral point, which is sensitive to a spectral feature primarily arising from the PxSH component. This had two consequences: (i) we monitored kinetics of PxSH with some contamination from PxSSPx signal; and (ii) we lost the information about PxSSPx kinetics. Was this loss of information significant? We did not find in the literature a detailed comparison of in vivo kinetics for both the disulfide-linked dinitroxide and the cleaved monomeric nitroxides. Existing studies did not include the complete analysis of the spectral shapes, but instead focus on the spectral features of the monomeric form[4,22]. Therefore, the approach used in the present study may be deemed acceptable until 4D imaging speed is accelerated by ~30-fold to enable the kinetics of cleavage to be fully characterized.

Quantitative GSH measurements

One of the factors that can affect accuracy of RS EPR imaging of thiol redox status is the consumption of cellular thiols due to reaction with spin probe, which would cause [RSH] to decline during the course of the experiment. The spin probe concentration as reported by imaging was 3 – 7 mM. Therefore, spin probe concentration was comparable to [RSH], which challenges the kinetic model used in this study. Declining [RSH] consequent to RSH consumption would lead to under-estimation of the cleavage rate constant. Accounting for the [RSH] depletion will require kinetic model considerably more complicated than the one presented in this study.

Another important factor that will affect the accuracy of thiol concentration measurements is pH. The fraction of thiol that exists as the nucleophilic thiolate species and contributes to PxSSPx cleavage is pH-dependent. Taking GSH as a specific example, a shift in pH from 7.2 by ±0.1 changes the concentration of the nucleophilic species by > 20% (see Fig. S1 and explanatory text in Supporting Information). Because thiol concentration is much higher inside cells than outside, cleavage is expected to be principally an intracellular process. Furthermore, acidification of the extracellular compartment in tumors means that what little extracellular thiol exists is essentially 100% in the non-nucleophilic form, and thus ineffective in cleavage. Therefore, it is safe to conclude that cleavage of the disulfide-linked spin probe occurs intracellularly. Although intracellular pH in tumor cells is typically found to be close to 7.2, any intracellular pH shift would nonetheless affect the estimated intracellular thiol concentration. Knowledge of the actual intracellular pH would thus improve thiol quantitation[23]. Availability of pH sensitive spin probes makes quantitative GSH measurement highly possible. A potentially desirable option is a dual-function probe that simultaneous yields information on pH and thiol redox status, as has been proposed[21].

4. Summary

In this work, we apply RS EPR for rapid 3-dimensional spatial imaging to obtain in vivo images of thiol redox status, specifically the estimation of intracellular thiol concentration in vivo. This technology enabled remarkably fast (30 second) 3D images and enabled resolution of kinetic processes occurring on the 100-second time scale. Using PxSSPx spin probe we imaged thiol content in mouse tumors and demonstrated sensitivity of our methodology to alterations of intracellular thiol concentration. The work represents the first success in achieving kinetically resolved thiol redox images on the physiologically relevant timescales. It also points out the enabling capability of RS EPR imaging.

5. Experimental

5.1 Instrumentation

A Rapid Scan RF bridge redesigned from a cw bridge[24] to have higher dynamic range and equipped with higher power 1W RF amplifier (ZHL-1A, Mini-Circuits, Brooklyn, NY) was used. We used a modified version of transmission bimodal cross-wire resonator[25] with the RF shield installed between the magnetic field scan coils and resonator, demonstrated to reduce baseline through long experience at the University of Chicago. The RF shield was

wound using 20 gauge wire to avoid induction of eddy currents and covered with conducting silver paint. A resonated magnetic field sweep driver was used to generate sinusoidal sweep[26]. The gradient and magnetic field system is described elsewhere[27]. SpecMan4EPR software version 2.1 controlled the imager[28]. The signals were filtered using Model 3955 filter (Kron-Hite, Brockton, MA) and detected using Acqiris AP235 (Keysight, Santa Rosa, CA) digitizer and averager.

For imaging we used 260 mW of RF power. The isolation of the excitation and detection portions of the bimodal resonator exceeding 55 dB was sufficient to keep the low noise amplifier in the linear regime. Each time trace acquired with 100 ns dwell time contained about 5 periods of rapid scan signal. 15000 traces were averaged for each spectrum. Scan frequency of 3.26 kHz and scan width of 7 mT was used for all measurements.

5.2. Rapid Scan imaging protocols

A filtered back projection (FBP) imaging protocol with 12×12 spatial angles (equal solid angle sampling) was used[29]. 94 projections and 2 zero gradient traces were acquired for each image. Zero traces were used to establish scanning and RF frequency phases. After deconvolution[30,31], parts of rapid scan traces used for reconstruction were down-sampled to FBP requirements[29]. Only the absorption signal component was used. 32×32×32 spectral-spatial images obtained upon FBP reconstruction were stacked together and each voxel intensity was fitted to Eq. 4 using MATLAB non-linear optimization routine. Only data above 15 % amplitude threshold were displayed and used for statistics.

5.3. Spin probe

1,6-bis([$^{2}H_{15}$,^{15}N]2,2,5,5-tetramethylpyrrolidin-1-oxyl-3-carboxamido)-3,4-dithiahexane (PxSSPx) was synthesized by published procedures[4]; its solubility in water is 35.0 ± 0.9 mM. A 20 mM solution was prepared in PBS containing 5% ethanol for intratumoral injection. The solution was injected through 30G needles in 2 parallel tracks. Injection was completed in < 5 s.

5.4. EPR spectra simulations

EPR spectra of PxSSPx and its cleaved, monomeric product were simulated using Easyspin software (www.easyspin.org). The complexity of multiple conformations of PxSSPx in solution was ignored because the simulation aimed to aid spectral decomposition rather than to obtain precise simulation parameters.

5.5. Nonlinear least-squares fitting of kinetic model

Standard nonlinear least-squares techniques were used to fit the kinetic model (Eqns 3 and 4) to the data. Fitting of Eqn 4 is straightforward. For the purpose of curve fitting, Eqn 3 was written in the equivalent form, $S_{\mathrm{PxSSPx}}=S^{0}_{\mathrm{PxSSPx}}e^{-k^{\mathrm{obs}}t}e^{-k^{\mathrm{clr}}t}$ to allow adjustment of the two rate constants. To test the robustness of fit, each kinetic data set was used to generate three separate data subsets: 1) the set of odd-index data, 2) the set of even-index data, and 3) the intact full data set. The appropriate kinetic equation (3 or 4) was fit to the three data subsets, and the three corresponding values of the rate constants (k^{obs} or k^{clr}) were used to compute a

mean and standard deviation (*s*). Generally, fits to Eqn 4 were more less variable, with *s* being 1 – 16% of the mean rate constant, whereas fits to Eqn 3 showed greater variability, with *s* ranging from ~3% to being comparable to the magnitude of the mean rate constant. This greater variability is not surprising because in Eqn 3, k^{obs} and k^{clr} are not truly independent and thus are more sensitive to shifts in the data set (i.e., whether the odd-indexed, even-index, or full data set is being fit). From the mean rate constants and their standard deviations obtained by fitting Eqns 3 and 4, $k_j^i \pm s_j^i (i=\mathrm{obs, clr}; j=3, 4)$, the final weighted average rate constant ($\overline{k^l}$) and estimated error ($\overline{s^l}$) were computed: $\overline{k^l}=\frac{\Sigma_j \left(k_j^i/s_j^{i^2}\right)}{\Sigma_j \left(1/s_j^{i^2}\right)}$ and $\overline{s^l}=\frac{1}{\Sigma_j \left(1/s_j^{i^2}\right)}$. The value of the parameter *a* in Eqn 4 was obtained analogously. OriginPro software (OriginLab Corp. Nothampton, MA) was used for curve fitting analysis.

5.6. Animal preparation and imaging protocol

FSa fibrosarcoma cells (2×10^5 – 10^6 cells) were injected intramuscularly into the right gastrocnemius muscle of 6 – 8 week old female C3H/HeN mice (Harlan Sprague-Dawley, Indianapolis, IN). The tumor was grown to 8 – 10 mm mean dimension. During the imaging preparations and actual imaging, the mouse inhaled a 1.0 – 2.0% isoflurane atmosphere adjusted to maintain steady sleep. The mouse's rectal and surface abdominal temperatures were monitored. IR radiant heating or external fan were adjusted to maintain the mouse's core temperature within the range from 36 °C to 38 °C. The general condition of the animals and the depth of anesthesia were optimized based on breathing pattern, maintained at 100 BPM. The tumor was immobilized in the resonator by a cast of vinyl polysiloxane dental impression material (GC Dental Products, Kasugai, Japan)[32]. For the purpose of EPR and MRI image registration, 3 fiducials were placed into the cast. After the second EPR image mice were sacrificed, and T2-weighed anatomical MRI enabled tumor localization. A total of 2.5 mg (100 mg/Kg, 200 μl of 20 mM solution) of the PxSSPx spin probe was injected in each animal; 8 animals were imaged. In addition we have tested two animals with injections of 5 mM and 10 mM solutions. The former did not permit imaging due to low SNR, while the 10 mM injection gave results similar to those obtained with 20 mM injection.

To change the tumor thiol redox state, L-buthionine sulfoximine (BSO), (THERMO SCI ACROS, Geel, Belgium) was applied as follows: The initial dose consisted of two injections, a 5 mg/kg BW ip injection (saline solution), and a 1 ml of 4 mM BSO solution sc injection. The animal was then allowed to recover from anesthesia overnight with a source of drinking water available ad libitum containing 20mM BSO. 18 h after first BSO application a second BSO dose was given as 5 mg/kg BW ip injection (saline solution). The second EPR imaging session was completed 24 h after first BSO injection.

All animal experiments were done according to the USPHS “Policy on Humane Care and Use of Laboratory Animals,” and the protocols were approved by the University Of Chicago Institutional Animal Care and Use Committee (ACUP No. 71697). The University of Chicago Animal Resources Center is an Association for Assessment and Accreditation of Laboratory Animal Care–approved animal care facility.

Supplementary Material

Refer to Web version on PubMed Central for supplementary material.

Acknowledgments

This work was supported by NIH grants P41 EB002034, R01 CA098575, R21 EB022775. GM056481, U54GM104942, R50 CA211408 and K25 EB016040.

References

1. Vaupel P, Hockel M. Blood supply, oxygenation status and metabolic micromilieu of breast cancers: characterization and therapeutic relevance. Int J Oncol. 2000; 17:869–879. [PubMed: 11029486]
2. Wardman P. Chemical radiosensitizers for use in radiotherapy. Clin Oncol (R Coll Radiol). 2007; 19:397–417. [PubMed: 17478086]
3. Brizel DM, Wasserman TH, Henke M, et al. Phase III randomized trial of amifostine as a radioprotector in head and neck cancer. J Clin Oncol. 2000; 18:3339–3345. [PubMed: 11013273]
4. Legenzov EA, Sims SJ, Dirda NDA, Rosen GM, Kao JPY. Disulfide-Linked Dinitroxides for Monitoring Cellular Thiol Redox Status through Electron Paramagnetic Resonance Spectroscopy. Biochemistry-Us. 2015; 54:6973–6982.
5. Bailey KM, Wojtkowiak JW, Hashim AI, Gillies RJ. Targeting the metabolic microenvironment of tumors. Adv Pharmacol. 2012; 65:63–107. [PubMed: 22959024]
6. Elas M, Ahn KH, Parasca A, et al. Electron paramagnetic resonance oxygen images correlate spatially and quantitatively with Oxylite oxygen measurements. Clin Cancer Res. 2006; 12:4209–4217. [PubMed: 16857793]
7. Elas M, Hleihel D, Barth ED, et al. Where it's at really matters: in situ in vivo vascular endothelial growth factor spatially correlates with electron paramagnetic resonance pO2 images in tumors of living mice. Mol Imaging Biol. 2011; 13:1107–1113. [PubMed: 20960236]
8. Dhimitruka I, Bobko AA, Hadad CM, Zweier JL, Khramtsov VV. Synthesis and characterization of amino derivatives of persistent trityl radicals as dual function pH and oxygen paramagnetic probes. J Am Chem Soc. 2008; 130:10780–10787. [PubMed: 18636723]
9. Samouilov A, Efimova OV, Bobko AA, et al. In vivo proton-electron double-resonance imaging of extracellular tumor pH using an advanced nitroxide probe. Anal Chem. 2014; 86:1045–1052. [PubMed: 24372284]
10. Meister A, Anderson ME. Glutathione. Annu Rev Biochem. 1983; 52:711–760. [PubMed: 6137189]
11. Messina JP, Lawrence DA. Cell cycle progression of glutathione-depleted human peripheral blood mononuclear cells is inhibited at S phase. J Immunol. 1989; 143:1974–1981. [PubMed: 2789253]
12. Lu SC, Ge JL. Loss of suppression of GSH synthesis at low cell density in primary cultures of rat hepatocytes. Am J Physiol. 1992; 263:C1181–C1189. [PubMed: 1476163]
13. Margis R, Dunand C, Teixeira FK, Margis-Pinheiro M. Glutathione peroxidase family - an evolutionary overview. FEBS J. 2008; 275:3959–3970. [PubMed: 18616466]
14. Prohaska JR. The glutathione peroxidase activity of glutathione S-transferases. Biochim Biophys Acta. 1980; 611:87–98. [PubMed: 7350921]
15. Mitchell JB, Russo A. The role of glutathione in radiation and drug induced cytotoxicity. Br J Cancer Suppl. 1987; 8:96–104. [PubMed: 3307879]
16. Wu JH, Batist G. Glutathione and glutathione analogues; therapeutic potentials. Biochim Biophys Acta. 2013; 1830:3350–3353. [PubMed: 23201199]
17. Elajaili H, Biller JR, Rosen GM, et al. Imaging disulfide dinitroxides at 250MHz to monitor thiol redox status. J Magn Reson. 2015; 260:77–82. [PubMed: 26415686]
18. Griffith OW. Mechanism of action, metabolism, and toxicity of buthionine sulfoximine and its higher homologs, potent inhibitors of glutathione synthesis. J Biol Chem. 1982; 257:13704–13712. [PubMed: 6128339]

19. Eaton SS, Quine RW, Tseitlin M, Mitchell DG, Rinard GA, Eaton GR. Rapid-Scan Electron Paramagnetic Resonance. Handbook of Multifrequency Electron Paramagnetic Resonance: Data and Techniques: Wiley-VCH Verlag. 2014:3–67.
20. Joshi JP, Ballard JR, Rinard GA, Quine RW, Eaton SS, Eaton GR. Rapid-scan EPR with triangular scans and fourier deconvolution to recover the slow-scan spectrum. J Magn Reson. 2005; 175:44–51. [PubMed: 15949747]
21. Bobko AA, Eubank TD, Voorhees JL, et al. In vivo monitoring of pH, redox status, and glutathione using L-band EPR for assessment of therapeutic effectiveness in solid tumors. Magnet Reson Med. 2012; 67:1827–1836.
22. Bobko AA, Dhimitruka I, Komarov DA, Khramtsov VV. Dual-Function pH and Oxygen Phosphonated Trityl Probe. Anal Chem. 2012; 84:6054–6060. [PubMed: 22703565]
23. Khramtsov VV, Yelinova VI, Glazachev Yu I, Reznikov VA, Zimmer G. Quantitative determination and reversible modification of thiols using imidazolidine biradical disulfide label. J Biochem Biophys Methods. 1997; 35:115–128. [PubMed: 9350517]
24. Quine RW, Rinard GA, Eaton SS, Eaton GR. A pulsed and continuous wave 250 MHz electron paramagnetic resonance spectrometer. Concept Magnetic Res. 2002; 15:59–91.
25. Rinard GA, Quine RW, Biller JR, Eaton GR. A Wire-Crossed-Loop Resonator for Rapid Scan EPR. Conc Magn Reson B. 2010; 37B:86–91.
26. Quine RW, Mitchell DG, Tseitlin M, Eaton SS, Eaton GR. A resonated coil driver for rapid scan EPR. Conc Magn Reson B. 2012; 41B:95–110.
27. Rinard GA, Quine RW, Eaton GR, et al. Magnet and gradient coil system for low-field EPR imaging. Concept Magnetic Res. 2002; 15:51–58.
28. Epel B, Gromov I, Stoll S, Schweiger A, Goldfarb D. Spectrometer manager: A versatile control software for pulse EPR spectrometers. Conc Magn Reson B. 2005; 26B:36–45.
29. Ahn KH, Halpern HJ. Spatially uniform sampling in 4-D EPR spectral-spatial imaging. J Magn Reson. 2007; 185:152–158. [PubMed: 17197215]
30. Tseitlin M, Mitchell DG, Eaton SS, Eaton GR. Corrections for sinusoidal background and non-orthogonality of signal channels in sinusoidal rapid magnetic field scans. J Magn Reson. 2012; 223:80–84. [PubMed: 22967891]
31. Tseitlin M, Rinard GA, Quine RW, Eaton SS, Eaton GR. Deconvolution of sinusoidal rapid EPR scans. J Magn Reson. 2011; 208:279–283. [PubMed: 21163677]
32. Haney CR, Fan X, Parasca AD, Karczmar GS, Halpern HJ, Pelizzari CA. Immobilization using dental material casts facilitates accurate serial and multimodality small animal imaging. Conc Magn Reson B. 2008; 33B:138–144.

Highlights

- Thiol redox status imaging using EPR
- Rapid Scan EPR imaging in vivo

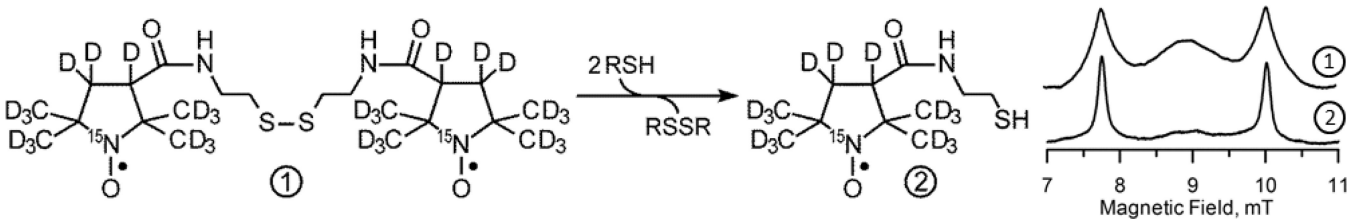

Figure 1.

Left. Schematic of the reaction of the disulfide-dinitroxide probe PxSSPx (1) with a thiol (RSH), leading to cleaved monomeric products, PxSH (2). Right. 251.1 MHz *in vitro* rapid-scan EPR spectra of PxSSPx (1) and PxSH (2) after cleavage of PxSSPx by RSH.

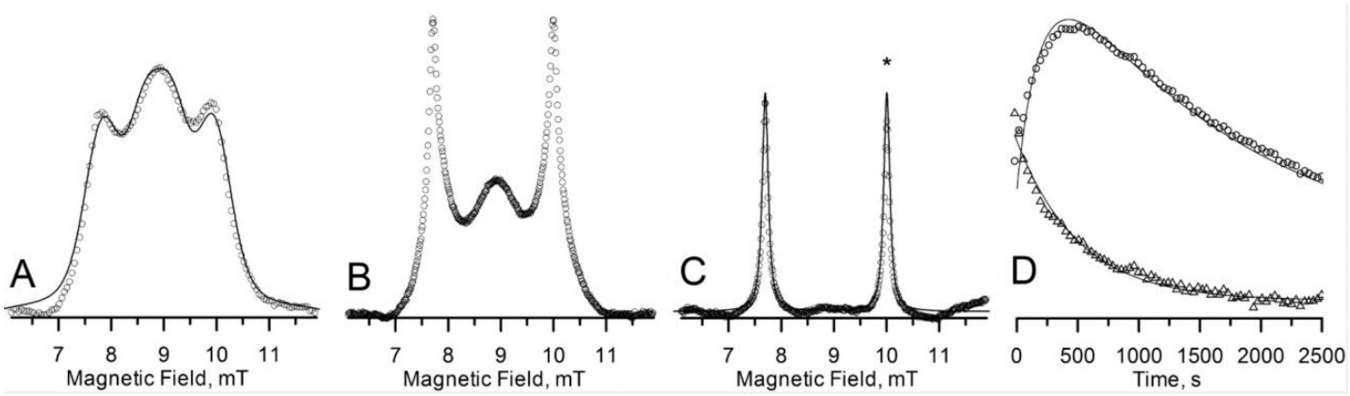

Figure 2.

250.8 MHz rapid-scan spectra of PxSSPx after injection into a tumor in vivo. Relative amplitudes are preserved. A. Immediately after injection. Circles represent data; solid line is simulated spectrum with ^{15}N hfi A = 2.04 mT and exchange coupling J = 110 MHz. B. At 175 s post-injection. C. At 1850 s post-injection. Solid line is simulated spectrum with 15N hfi A = 2.31 mT. D. Time dependence of the PxSSPx (triangles) and PxSH (circles) spin numbers; solid curves are simulations with $k_1^{\mathrm{obs}}=1.85\cdot 10^{-3}\mathrm{s}^{-1}$, $k_2^{\mathrm{obs}}=6.65\cdot 10^{-3}\mathrm{s}^{-1}$ and $k_2^{\mathrm{clr}}=0.39\cdot 10^{-3}\mathrm{s}^{-1}$ (see main text for details).

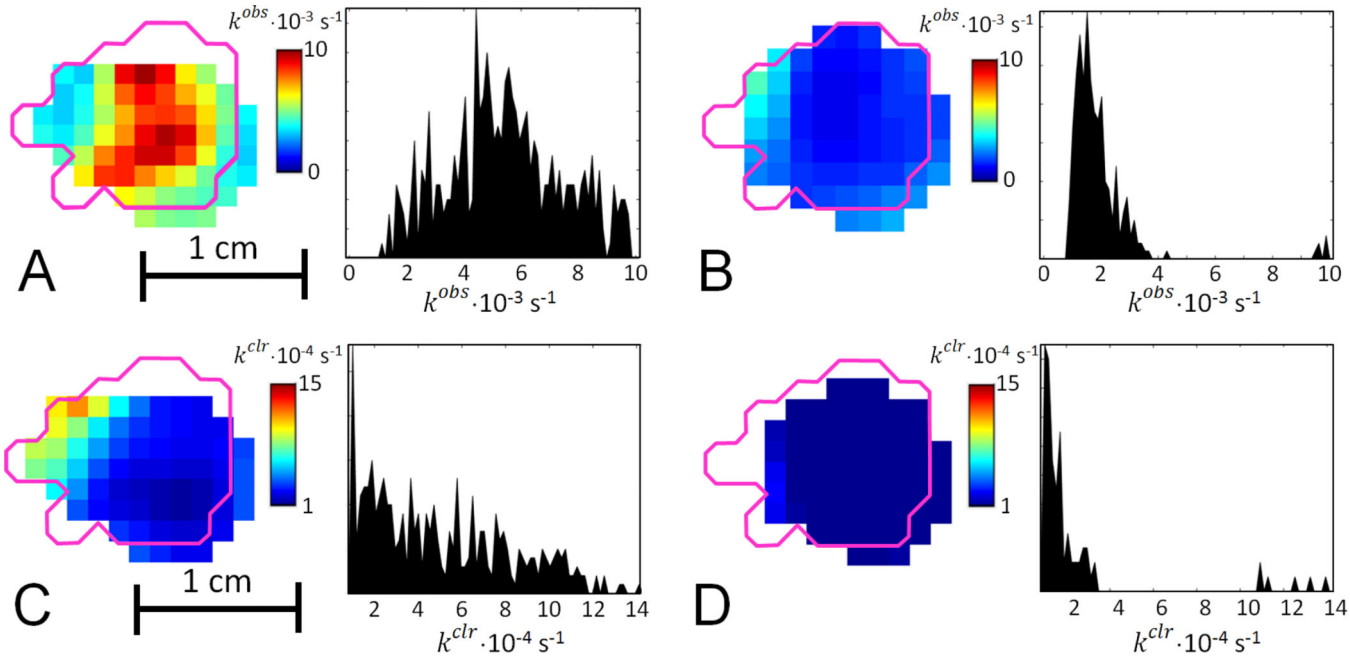

Figure 3.

Sagittal slices and histograms of cleavage rate $\boldsymbol{k^{obs}}$ images in FSa tumor A. before; and B. 24 h after application of BSO. Magenta outline shows the tumor border as obtained from a registered MRI image. The histogram shows $\boldsymbol{k^{obs}}$ in all voxels of the tumor. Sagittal slices and histograms of clearance rate $\boldsymbol{k^{clr}}$, images in FSa tumor C. before; and D. 24 h after application of BSO. Magenta outline shows the tumor border as obtained from a registered MRI image. The histogram shows $\boldsymbol{k^{obs}}$, in all voxels of the tumor.

Table 1

Kinetic data for three representative animals*

Animal	a		k^{obs}, 10^{-3} s^{-1}		k^{clr}, 10^{-3} s^{-1}	
	Control	BSO	Control	BSO	Control	BSO
1	0.39 (0.006)	0.46 (0.01)	3.0 (0.06)	1.6 (0.07)	0.39 (0.007)	0.073 (0.04)
2	0.48 (0.01)	0.34 (0.001)	2.0 (0.09)	1.1 (0.01)	0.12 (0.03)	0.17 (0.002)
3	0.39 (0.006)	0.46 (0.01)	3.6 (0.1)	1.5 (0.03)	0.66 (0.03)	0.32 (0.008)

*Values in parentheses are estimated standard errors.